Journal of Advanced Ceramics
2020, **9**(4): 403–412
https://doi.org/10.1007/s40145-020-0380-y

ISSN 2226-4108
CN 10-1154/TQ

Research Article

Direct ink writing of continuous SiO_2 fiber reinforced wave-transparent ceramics

Zhe ZHAO[a,b], Guoxiang ZHOU[a,b], Zhihua YANG[a,b,c,*], Xianqi CAO[d], Dechang JIA[a,b], Yu ZHOU[a,b]

[a]*Key Laboratory of Advanced Structural-Functional Integration Materials & Green Manufacturing Technology*, *Harbin Institute of Technology*, *Harbin 150001*, *China*
[b]*Institute for Advanced Ceramics*, *School of Materials Science and Engineering*, *Harbin Institute of Technology*, *Harbin 150080*, *China*
[c]*State Key Laboratory of Advanced Welding and Joining*, *Harbin Institute of Technology*, *Harbin 150001*, *China*
[d]*Institute of Petrochemistry Heilongjiang Academy of Science*, *Harbin 150001*, *China*

Received: December 6, 2019; Revised: April 8, 2020; Accepted: April 15, 2020

Abstract: This article reports the first example of 3D printed continuous SiO_2 fiber reinforced wave-transparent ceramic composites via an adaptation of direct ink writing technology to improve the mechanical and dielectric properties of ceramics. The ceramic inks showed good printability by adding nano-SiO_2 powder. The effective continuous fiber-reinforced printing progress was achieved through the design and optimization of the coaxial needle structures by finite element simulation. After printing, the continuous fibers were evenly and continuously distributed in the matrix ceramics and the high molding precision for fiber reinforced composite was kept. It is demonstrated that 10 vol% continuous SiO_2 fiber improved the bending strength of ceramics by about 27% better than that of the ceramics without fiber and the dielectric performance has also been greatly improved. The novel method unravels the potential of direct ink writing of continuous fiber reinforced wave-transparent ceramics with complex structures and improved properties.

Keywords: 3D printing; continuous fiber reinforced; rheology; dielectric properties

1 Introduction

Phosphate is a kind of low dielectric constant ceramics applied to high-temperature structural and wave-transparent applications in aerospace and other fields, owing to its impressive properties such as mechanical strength, thermal stability at high temperature, and low cost [1–3]. However, the applicability of phosphates was limited on account of their low toughness and the inefficiency of molding [4–6]. Fiber reinforcement, including short fiber and continuous fiber reinforcement, is a toughening method commonly used for ceramic materials. With a better effect, long fiber reinforcement is considered to be the most ideal toughening method for ceramic materials. A traditional process for preparing continuous fiber reinforced ceramics is maceration [7–9], which may do harm to fibers due to the acidity of the phosphate solution, and is not conducive to the formation of complex structures. 3D printing can

* Corresponding author.
E-mail: zhyang@hit.edu.cn

theoretically be used for rapid prototyping of complex structures by layer-by-layer stacking of materials [10–13] with almost no mechanical processing after molding, thereby simplifying the production process and shortening the production cycle.

3D printing technology of ceramics mainly includes powder bed techniques [14,15], laser selective sintering [16,17], selective laser melting [18,19], direct ink writing (DIW) [20–22], ink-jet printing [23–26], stereolithography [27,28], and the like. Fiber-reinforced 3D printing technology is a good choice for ceramic materials with limited material toughness and complex structural forming requirements, but the application of 3D printing in continuous fiber-reinforced ceramics is limited. Except for 3D printed short fiber reinforced ceramics [29], most of the continuous fiber reinforced materials reported so far were prepared by fused deposition modeling (FDM) [30–33], in which the raw materials were almost all polymer materials and carbon fibers. Stepashkin *et al.* [34], for instance, have reported a novel FDM methodology for manufacturing CF-PEEK composites using a customized printer. However, such a hot-melt extrusion technique method can only be employed on thermoplastic materials that will fail at high temperature. Besides, although carbon fiber has good mechanical properties, it is not suitable for a reinforcement of wave-transparent materials. There is still lack of an effective and convenient technology for the integrated manufacturing of continuous fiber reinforced materials, especially for the wave-transparent ceramic materials. Comparing to FDM, the DIW technology has the advantages of low cost, high molding efficiency, and wide range of applications. However, DIW technology is only applied to short-cut fiber reinforced composites currently [29,35]. Considering the application of DIW technology, controlling of rheological properties of ceramic ink is the most critical issue. As reported by Lewis, who took the lead in successfully printing complex three-dimensional ceramic structures using water-based colloidal slurry [36], the rheological properties of the inks were depended on the interparticle forces. When it comes to the continuous fiber reinforced phosphate composites, the rheology properties of phosphate inks are the primary problem to be studied. Compton and Lewis [37] achieved the formation of high aspect ratio fiber oriented reinforced composites by extrusion 3D printing technology. During the experiment, an epoxy-based ink was prepared using Epon 826 epoxy phosphate, nano-clay tablets, and dimethyl methyl phosphate. Besides, for extrusion 3D printing, the structure of the nozzle is the other key issue for the preparation of continuous fiber reinforced ceramics, and corresponding attempts [38,39] have been made in response to this problem. Apart from the difficulties mentioned before, the lack of an effective DIW based 3D printing technology for the integrated manufacturing of continuous fiber reinforced ceramic materials is one of the greatest obstacles that restricts the development of ceramic performance. Thus there have been almost no reports on the applications of DIW on continuous fiber reinforced ceramic at home and abroad so far, especially wave-transparent ceramic materials.

Here we propose a DIW based 3D printing method for the integrated manufacturing of continuous fiber reinforced wave-transparent ceramics by using the viscosity and friction of the inks as the power source of the continuous fiber extrusion for the first time. For purpose of ensuring the smooth and continuous extrusion of the fiber, the structural design of the coaxial needle and the rheological property regulation of the ink have become the core issues of this work. In the case of continuous SiO_2 fiber being used as the enhanced phase, and SiO_2/phosphate material as matrix material, through the design of the nozzle, together with the finite element simulation of flow fields internal, the integrated molding of the continuous SiO_2 fiber reinforced SiO_2/phosphate composites are achieved finally.

2 Experimental details

2. 1 Materials and preparation of ceramic inks

The raw material J-303 was offered by Institute of Petrochemistry Heilongjiang Academy of Science, which was actually a kind of phosphate adhesive. Nano-SiO_2 powder (99% purity, Xianfeng Nano Technology Co. Ltd., Nanjing, China) was employed as a rheology modifier in the ceramic inks used for DIW method in this study. Table 1 lists the initial compositions for the synthesis of wave-transparent ceramic inks. Phosphate was firstly mixed with nano-SiO_2 powder, and a mechanical mixing progress was employed at 1000 r/min for 20 min to uniformly disperse nano-SiO_2 powder in phosphate. Then ceramic inks with a stabilized rheological property could be prepared in this way. The obtained ceramic inks will be molded together with 10 vol% continuous SiO_2 fibers (diameter of a single fiber is about 6.5 μm, Feilihua Quartz Glass Co., Ltd., Hubei,

Table 1 Composition of wave-transparent ceramic inks
(Unit: wt%)

Sample	Phosphate inks	Nano-SiO_2 powder
1	96.32	3.68
2	94.95	5.05
3	92.49	7.51
4	90.36	9.64
5	88.24	11.76

China) by direct ink writing 3D printing technology.

2. 2 3D printing

The schematic diagram of continuous fiber reinforced 3D printing process was shown in Fig. 1. 3D printing progress was carried out by a modified commercial 3D printer (Ultimaker extend 2+) at room temperature. Before printing, the continuous fiber was passed through the fiber channel and ceramic inks were loaded into a dispensing syringe which was connected with a dispensing machine (Nordson EFD) and an air pump. For the integrated molding of the continuous fiber and ceramic inks, a coaxial needle structure was designed and fabricated. When 3D printing was performed, the inks were extruded into the printing needle and the fibers were wrapped in the inks and finally formed as a core shell structure as shown in Fig. 1. To verify the feasibility of this particular design, a process of finite element simulation was carried out. Before the simulation, a three-dimensional model of the coaxial needle was established by AutoCAD according to the preset parameter conditions. Then the built 3D model was meshed using a free tetrahedral mesh and imported into COMSOL to analyze the distribution of the flow velocity and shear rate of the ink. The finite element parameters were as follows: density was 1200 kg/m^3; dynamic viscosity was determined to be 10,000 Pa·s; given external pressure was loaded on the entrance of printing needle was 0.1 MPa.

2. 3 Characterization

To cater to the performance of the 3D printer, the rheological properties of the SiO_2/phosphate inks, which had a direct impact on the accuracy of 3D printing, were characterized by Discovery Hybrid Rheometer HR-1 (TA Instruments) at room temperature with an 80 mm flat plate geometry and a gap of 2000 μm. The stress sweep tested from 3 to 3×10^4 Pa at a constant frequency of 1 Hz was conducted to record the storage modulus and loss modulus variations as a function of sweep stress. And the flow sweeps tested from 10^{-1} to 10^1 s^{-1} were performed to record the apparent viscosity as a function of shear rates.

The 3D printed green body was dried at room temperature for 24 h and then cured at 180 ℃ for 12 h with a heating rate of 5 ℃/min. The microstructure of samples was observed by scanning electron microscopy (SEM) after gold sputtering. The apparent porosity (π) at ambient temperature was measured by the Vacuum method. The formula for the apparent density is

$$\pi = \frac{m_3 - m_1}{m_3 - m_2} \times 100\% \quad (1)$$

where m_1 is the dry weight of sample in air (g), m_2 is the float weight of sample in distilled water (g), and m_3 is the wet weight of the sample, which is taken out of the distilled water (g). The samples above were weighed

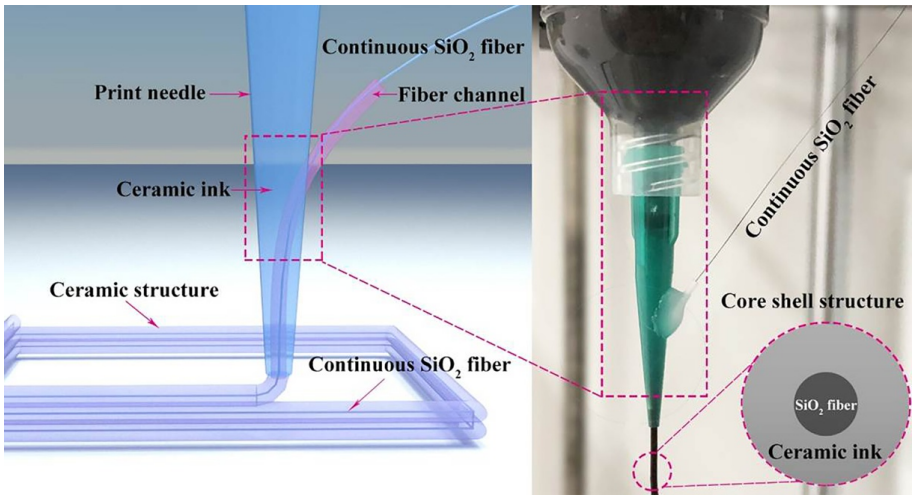

Fig. 1 Schematic illustration of 3D printing continuous fiber reinforced ceramics process.

using TG328A photoelectric analysis balance. Each sample is measured at least three times to average.

The bending strength (σ_f) was determined on an Instron-5569 electronic universal testing machine with a loading rate of 0.5 mm/min by the three-point bending method at room temperature, and each sample was measured at least three times. To satisfy the requirements of the bending test, samples with a dimension of 3 mm × 4 mm × 25 mm were printed. Before the test, the pressure-receiving surface of the sample and its opposite surface were sanded to parallel. The formula of bending strength is

$$\sigma_f = \frac{3PL}{2BW^2} \tag{2}$$

where P is the maximum load before the sample fractures (N); L is the span of the test, which is 16 mm; B is the width of the sample (mm) and W is the height (mm). The dielectric properties at room temperature are characterized by dielectric constant and dielectric loss. American N2230A dielectric property testers were used to test at 8–20 Hz. The contents of nano-SiO_2 powder are used to study the effect on dielectric properties of materials.

3 Results and discussion

3. 1 Finite element simulation of coaxial needle

Compared with the carbon fiber commonly used in fiber-reinforced 3D printing [40], SiO_2 fiber is not strong enough to withstand the mechanical power. Therefore, a coaxial needle structure was designed (Fig. 1) to extrude the continuous fiber together with ceramic inks without additional power source. During the printing progress, the friction between ceramic inks and fibers was used as the continuous fiber extrusion power, so that the continuous fibers could be integrally formed and dragged by inks in the extrusion process. In this coaxial needle structure, the geometry structure and dimension have a significantly influence on the feasibility and stability of the printing progress. In order to optimize the geometry of the coaxial needle, a three-dimensional fluid-mechanics model was built by finite element simulation. The effects of the diameter of printing needle and the intersection position of printing needle and fiber channel on the continuous extrusion process of the fiber were studied by setting different parameters respectively. Through the distribution of the velocity and shearing rate of the printing inks, the printing fluency and the shear force that the continuous fiber born can be qualitatively evaluated. The global flow dynamics of a given needle geometry could be assessed effectively as well.

Figure 2 shows the simulation results of the internal fluid of coaxial needle. It can be observed that in the upper of the needle, where the given extrusion pressure is uniform and stable, the fluid flow velocity and shear rate show a regular increase. As the ceramic inks being pushed to the intersection of the printing needle and the fiber channel, it can be clearly seen that both the shear rate and velocity increase along the axial direction of the needle. What is more, at the outlet of the coaxial needle, the flow velocity and shear rate are the largest. Under this circumstance, ceramic inks can completely cover the continuous fiber and provide sufficient strength to bring it out. It can be obtained from Fig. 2(a) and Fig. 2(c) that the flow velocity and shear rate increase with the printing needle diameter increasing. Apparently, the larger the diameter of the printing needle, the smoother the continuous fiber extrusion during 3D printing. Considering the molding precision influence brought by the needle diameter, the diameter of 1.2 mm is selected as the printing needle while the external diameter of fiber channel is 0.51 mm. Similar conclusions can be drawn from Figs. 2(b) and 2(d) that the lower the intersection position of the printing needle and fiber channel, the easier the continuous fiber could be driven. Considering the operability of the experiment, the height of exit position is set to 5 mm, which is the minimum height that can be reached in this work.

Based on the above simulation results, the geometric characteristics of the coaxial needle have a direct influence on the 3D printing process of the continuous fiber reinforced ceramic. As a result, the feasibility of fabricating continuous fiber reinforced ceramic materials through DIW technology combined with the coaxial needle is demonstrated and optimized by the finite element simulation results above.

3. 2 Rheological properties of ceramic inks

To obtain 3D printed continuous fiber reinforced ceramics, printable ceramic inks should be prepared firstly. As mentioned before, the rheological properties of ceramic inks showed a critical impact on the molding accuracy during DIW 3D printing. The ability for a given ceramic ink formulation to be printable using a DIW process was in a large part depended on the static and flow

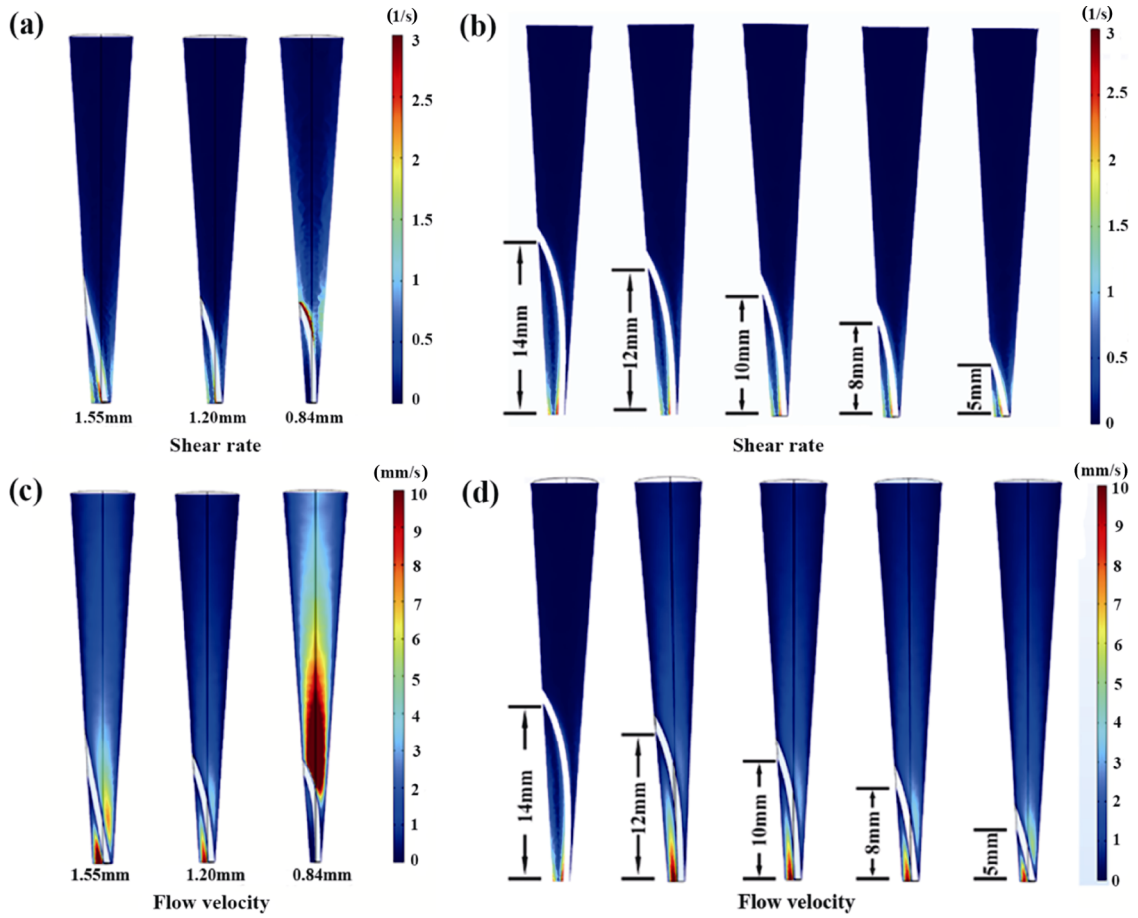

Fig. 2 Simulation results of the internal fluid of coaxial needle: (a, c) different diameters of the printing needle, (b, d) different intersection position of the printing needle and fiber channel.

rheology of the formulation. The rheological properties of the SiO_2/phosphate inks were analyzed using the rheometer. The increases in "static" viscosity (as shear rate→0) can be observed with the nano-SiO_2 powder adding as shown in Fig. 3(a). The nano-SiO_2 powder with a small particle size of 20 nm has a large specific surface area (140.21 m^2/g) and high surface energy, which make the particles unstable and tend to agglomeration. Meanwhile, increasing of nano-SiO_2 powder contents shortens the distance between these nanoparticles. According to the theory of colloidal science, the stability of colloid is closely related to the particle spacing—it will significantly reduce when the particles get closer to each other. Hence, increasing of nano-SiO_2 powder makes it much more easily for the nanoparticles to agglomerate. The aggregates of nano-SiO_2 would absorb more free water [41], so that the viscosity of ceramic inks increased with increasing nano-SiO_2 powder contents. Besides, it can be seen from Fig. 3(a) that the viscosity shows little change with the rise of shear rates when the content of nano-SiO_2 powder is 0, which indicates that the phosphate inks without nano-SiO_2 powders exhibit a characteristic of Newtonian fluid. Viscosity of the other inks decreased with the increase of shear rate, which is commonly called "shear thinning", showing a characteristic of non-Newtonian fluid. It can be speculated that the addition of nano-SiO_2 converts the original Newtonian fluid that is unsuitable for 3D printing into a non-Newtonian fluid. To verify this conjecture, the experimental data is compared with power-law fluid and Carreau fluid model, which is classical non-Newtonian fluid models, as shown in Fig. 3(c), manifesting that the SiO_2/phosphate composite system conforms to the classical Carreau fluid model as shown in Eq. (3) [27].

$$\mu = \mu_\infty + (\mu_0 - \mu_\infty)(1 + \lambda\gamma^2)^{(n-1)/2} \tag{3}$$

where μ_∞ is the viscosity of the fluid when the shear rate is infinite, determined to be 8000 Pa·s; μ_0 refers to the viscosity of the fluid when the shear rate is 0; γ is a shear rate and the constants λ, n were determined to be 42, 0.1, respectively.

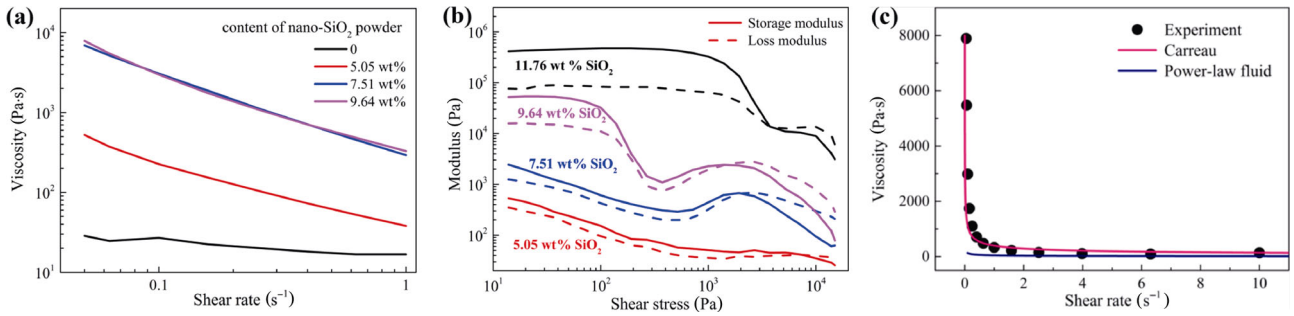

Fig. 3 Rheology properties of SiO_2/phosphate inks: (a) viscosity as a function of shear rate, (b) shear modulus as a function of shear stress, (c) comparison of experimental data and theoretical models.

Figure 3(b) shows that the loss modulus of the SiO_2/phosphate inks is bigger than the storage modulus at high shear stress. With the decreasing of the shear stress, both the storage modulus and the loss modulus increase, and the two modulus curves get an intersect point. After the intersection, the loss modulus is less than the storage modulus. The change in modulus meets the requirements of DIW 3D printing technology. In detail, the ceramic ink can be extruded from the printing nozzle in a liquid state under the pressure given by the 3D printing device and it is also able to form and maintain the printed structure in a solid state.

As stated previously, the addition of nano-SiO_2 powder showed a great improvement to the rheological properties of the phosphate inks. The comparatively high static viscosity supported the observation that the fluid rapidly relaxed at the point of extrusion and physically solidified on removal of the shearing force. And we have demonstrated that it is possible to print self-supporting structures by embellishing phosphate inks with nano-SiO_2 powder (Fig. 4). Significantly, it has been experimentally observed that if a phosphate ink without nano-SiO_2 powder was used for 3D printing with continuous fibers, the resulting system would not be extruded from the DIW nozzle under pressure. The inks and fibers will in fact phase separate, with the ink flowed through the static fiber phase in the nozzle assembly. It was observed that the higher viscosity nano-SiO_2 modified phosphate included significantly increased drag forces between the fiber and the ink and allowed the fiber phase to be effectively "carried" as a continuous component of the fluid matrix.

3. 3 3D printing of continuous fibers into ceramics

Through the design of coaxial needle and the regulation of the rheological properties of the SiO_2/phosphate ink, physical images of several complex structures are prepared by DIW 3D printing, as shown in Fig. 4. It is observed that complex ceramic structures like honeycomb and three-dimensional vertical and horizontal structures are all high-precision molded. The morphology of 3D printed samples is analyzed using SEM as shown in Figs. 4(d), 4(e), and 4(f), which presents the micromorphology inside the matrix wave-transparent ceramics and the microstructure of 3D printed structures at lap point and

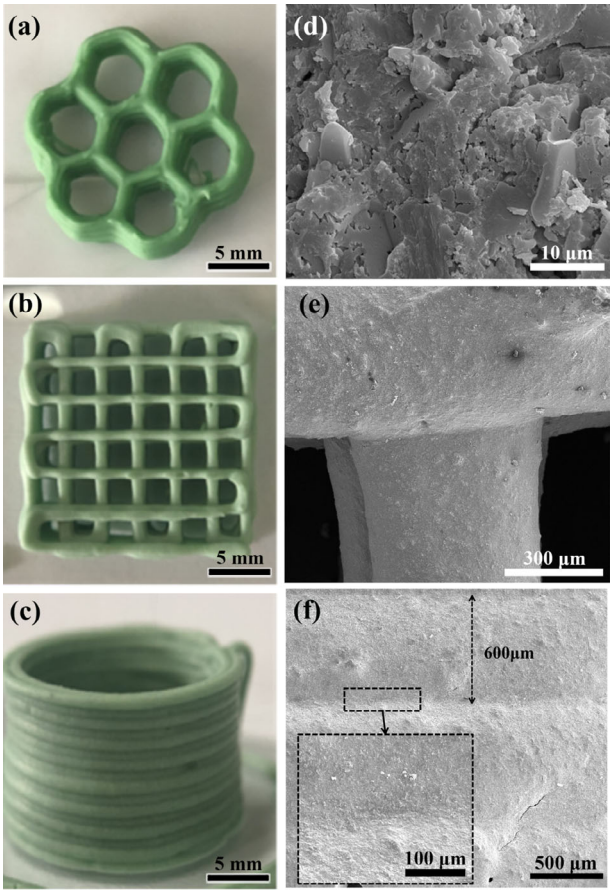

Fig. 4 Photos of 3D printed fiber-free samples. Physical photos: (a) honeycomb model, (b) three-dimensional model, (c) cylinder model. SEM images: (d) fracture surface, (e) lap point, (f) layers.

between layers, respectively. These complex structures have high modeling accuracy and can keep stable after 3D printing. Typical bulk structure and SEM images for continuous SiO_2 fiber reinforced SiO_2/phosphate composite printed using the coaxial needle structure are shown in Fig. 5. Comparing fiber-reinforced samples with fiber-free samples, it can be seen that the microstructure of the matrix wave-transparent ceramic materials does not change significantly, showing that the introduction of fibers has little effect on the curing of the ceramics. It can be observed from Figs. 5(b) and 5(c) that the fibers, distributing continuously and evenly, are wrapped in the ceramics, and the interface between the two is tightly combined. The dents left in the matrix ceramic after the fiber being pulled out can be clearly observed in Fig. 5(d), which is consistent with the fiber diameter. It can be inferred that through the coaxial needle designed in this work, combined with the regulation of ceramic inks, 3D printing of continuous fiber reinforced ceramics has been successfully realized, and the fibers are well dispersed in the matrix.

A comparison of the mechanical and dielectric properties between fiber-reinforced and fiber-free 3D printing samples is given in Fig. 6. Apparent porosity of the samples is all above 20% as shown in Fig. 6(a), which can be attributed to the pores generated during the curing process of ceramics at 180 ℃. The addition of continuous fibers reduces the apparent porosity of composites to a certain extent, indicating that continuous

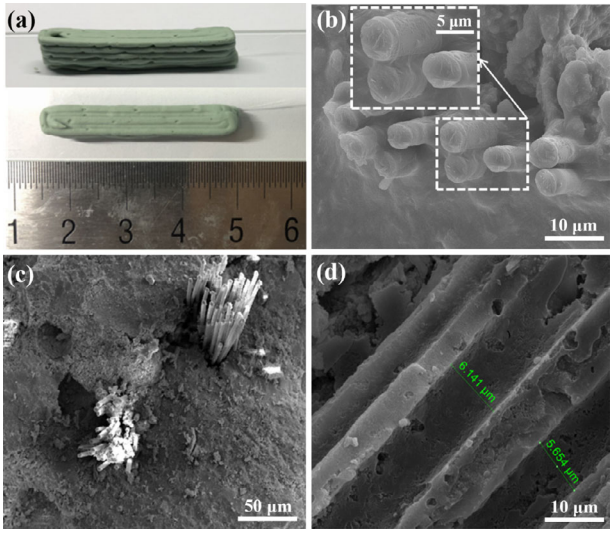

Fig. 5 Photos of 3D printed fiber-reinforced samples: (a) bulk of continuous SiO_2 fiber reinforced SiO_2/phosphate composite, (b–d) SEM images.

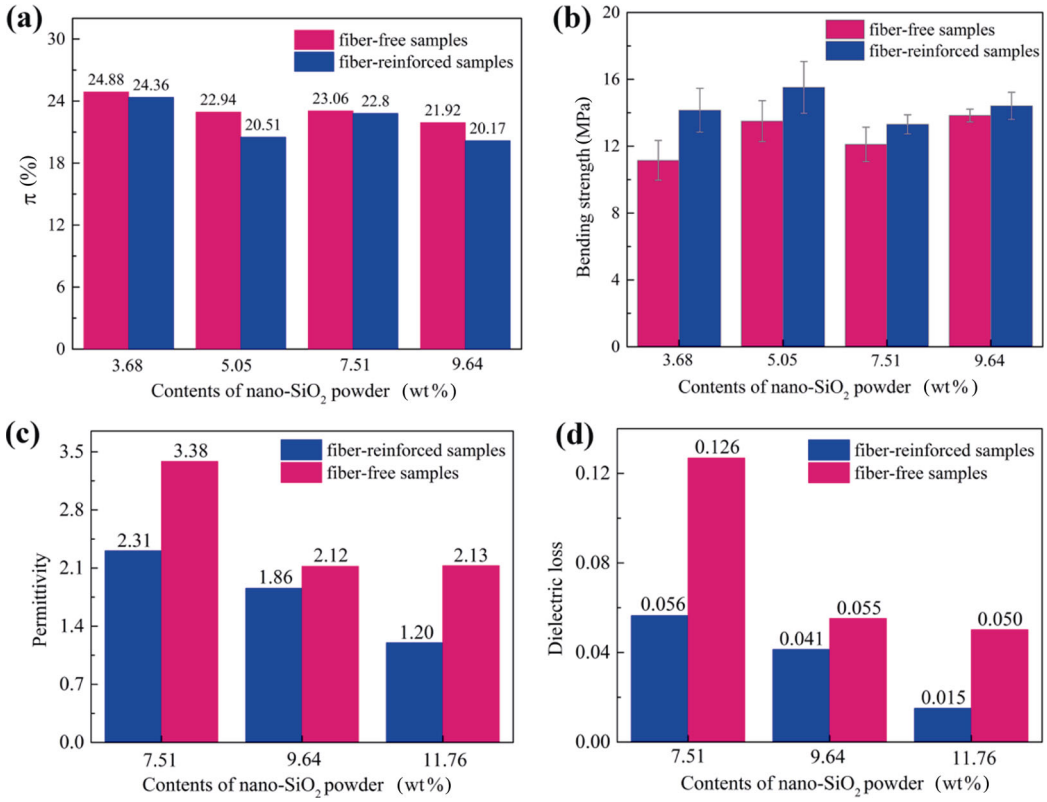

Fig. 6 Comparison of properties of samples with and without fiber reinforcement: (a) apparent porosity, (b) bending strength, (c) dielectric constant, (d) loss tangent.

fibers are well combined with ceramics. Correspondingly, samples with less pores exhibit a higher bending strength, as shown in Fig. 6(b), which implies that the mechanical response of the printed samples is relative to their apparent porosities. Comparing the two samples with a nano-SiO_2 powder content of 3.86 wt%, the apparent porosity of the fiber-reinforced sample is 24.36% while the fiber-free sample is 24.48%. The corresponding improvement in bending strength is approximately 27%, from 14.15±1.3 to 11.2±1.1 MPa, which indicates that except for apparent porosity, continuous fibers are the main reason for the improvement in the bending strength of the composites. In general, continuous fiber-reinforced 3D printing is proved to be effective in improving the mechanical properties of wave-transparent ceramics in this work. The continuous SiO_2 fibers and matrix ceramics are well bonded in the prepared samples, and it is demonstrated that 10 vol% continuous SiO_2 fibers improved the bending strength of ceramics by about 27% better than that of the ceramics without fiber. Although it is not a prominent improvement in mechanical properties compared with traditionally manufactured continuous SiO_2 fiber reinforced ceramics [42], DIW based 3D printing technology is still a promising way for the integrated manufacturing of continuous fiber reinforced ceramic materials with complex structures.

The continuous SiO_2 fiber and nano-SiO_2 powder added into matrix ceramics also bring obvious improvement on the dielectric properties to the composites due to their good dielectric performance. It can be seen from Figs. 6(c) and 6(d) that the dielectric properties are improved with the nano-SiO_2 powder adding, and when the content of nano-SiO_2 powder is 11.76 wt% and continuous SiO_2 fiber is 10 vol%, the dielectric constant of the continuous SiO_2 fiber reinforced SiO_2/phosphate composite material is 1.2, which is 43.4% lower than that of the matrix material. The loss tangent is 1.5×10^{-2}, which is 70% lower than the matrix. And it is worth mentioning that the dielectric constant of the obtained composites (1.2–2.3) is much lower than that prepared in the traditional way [43–45]. In addition to SiO_2 fiber and powder, the apparent porosity of the composite prepared in this work is relatively higher (more than 20%), and the dielectric constant of the air is 1. Thus the obtained composites showed better dielectric properties. Based on the above analysis, it can be entailed that continuous fiber reinforced wave-transparent ceramics can be well prepared through DIW 3D printing technology, and the continuous SiO_2 fiber can contribute to the performance of wave-transparent ceramics both in mechanical and dielectric properties.

4 Conclusions

In this work, continuous SiO_2 fiber reinforced SiO_2/phosphate composite was successfully fabricated by DIW technology and studied in terms of mechanical and dielectric properties. To realize the integrate molding of continuous fibers and wave-transparent ceramics, the rheological properties of the inks were regulated and the finite element simulation was performed to adjust the geometry of the coaxial needle. By mixing nano-SiO_2 powder with phosphates, the wave-transparent ceramic inks exhibit good rheological properties and printability for commercial DIW printers. The homogeneous-dispersed continuous fiber reinforced ceramic structures were obtained with improved dielectric properties and enhanced mechanical properties using DIW technology. The continuous SiO_2 fibers improved the bending strength of matrix ceramics by 27% with the 10 vol% content of continuous fiber. And when the content of nano-SiO_2 powder was 11.76 wt% and the continuous fiber was 10 vol%, the dielectric constant of the composite was 1.2 and dielectric loss tangent was 1.5×10^{-2}, which was 43.4% and 70% lower than the matrix itself, respectively. The novel method unravels the potential of DIW 3D printing technology for continuous fiber reinforced ceramics with complex structures and improved strength.

Acknowledgements

This work is supported by the National Key R&D Program of China (Nos. 2017YFB0310400 and 2017YFB0310402) and the National Natural Science Foundation of China (NSFC, No. 51972079).

References

[1] Barbosa VFF, MacKenzie KJD. Synthesis and thermal behaviour of potassium sialate geopolymers. *Mater Lett* 2003, **57**: 1477–1482.

[2] Deventer JSJV, Provis JL, Duxson P. Commercial progress in geopolymer concretes: Linking research to applications.

In Proceedings of the 1st International Conference on Advances in Chemically-Activated Materials, 2010: 22–27.

[3] Van Deventer JSJ, Provis JL, Duxson P. Technical and commercial progress in the adoption of geopolymer cement. *Miner Eng* 2012, **29**: 89–104.

[4] Fanelli AJ, Silvers RD, Frei WS, *et al*. New aqueous injection molding process for ceramic powders. *J Am Ceram Soc* 1989, **72**: 1833–1836.

[5] Travitzky N, Bonet A, Dermeik B, *et al*. Additive manufacturing of ceramic-based materials. *Adv Eng Mater* 2014, **16**: 729–754.

[6] Liu LP, Cui XM, He Y, *et al*. Study on the dielectric properties of phosphoric acid-based geopolymers. *Mater Sci Forum* 2010, **663–665**: 538–541.

[7] Deng SF, Wang CF, Zhou Y, *et al*. Preparation and characterization of fiber-reinforced aluminum phosphate/silica composites with interpenetrating phase structures. *Int J Appl Ceram Technol* 2011, **8**: 360–365.

[8] Hoshii S, Kojima A, Tamaki T, *et al*. Carbon fiber/ceramic composite using aluminum phosphate with different P/Al molar ratios. *J Mater Sci Lett* 2000, **19**: 557–560.

[9] Yang J, Lv Y, Zhang C, *et al.* Improvements of microwave transparent composites and aircraft radome. *Aerospace Materials & Technology* 2015, **45**: 6–9. (in Chinese)

[10] Elahinia M, Shayesteh Moghaddam N, Taheri Andani M, *et al*. Fabrication of NiTi through additive manufacturing: A review. *Prog Mater Sci* 2016, **83**: 630–663.

[11] Kumar A, Mandal S, Barui S, *et al*. Low temperature additive manufacturing of three dimensional scaffolds for bone-tissue engineering applications: Processing related challenges and property assessment. *Mat Sci Eng R: Rep* 2016, **103**: 1–39.

[12] Minas C, Carnelli D, Tervoort E, *et al*. 3D printing of emulsions and foams into hierarchical porous ceramics. *Adv Mater* 2016, **28**: 9993–9999.

[13] Tumbleston JR, Shirvanyants D, Ermoshkin N, *et al.* Continuous liquid interface production of 3D objects. *Science* 2015, **347**: 1349–1352.

[14] Butscher A, Bohner M, Doebelin N, *et al*. New depowdering-friendly designs for three-dimensional printing of calcium phosphate bone substitutes. *Acta Biomater* 2013, **9**: 9149–9158.

[15] Moon J, Grau JE, Knezevic V, *et al*. Ink-jet printing of binders for ceramic components. *J Am Ceram Soc* 2004, **85**: 755–762.

[16] Guo D, Li LT, Cai K, *et al*. Rapid prototyping of piezoelectric ceramics via selective laser sintering and gelcasting. *J Am Ceram Soc* 2004, **87**: 17–22.

[17] Liu K, Sun H, Shi Y, *et al*. Research on selective laser sintering of Kaolin-epoxy resin ceramic powders combined with cold isostatic pressing and sintering. *Ceram Int* 2016, **42**: 10711–10718.

[18] Shishkovsky I, Yadroitsev I, Bertrand P, *et al.* Alumina–zirconium ceramics synthesis by selective laser sintering/melting. *Appl Surf Sci* 2007, **254**: 966–970.

[19] Sing SL, Yeong WY, Wiria FE, *et al*. Direct selective laser sintering and melting of ceramics: A review. *Rapid Prototyp J* 2017, **23**: 611–623.

[20] Derby B. Additive manufacture of ceramics components by inkjet printing. *Engineering* 2015, **1**: 113–123.

[21] Maleksaeedi S, Eng H, Wiria FE, *et al*. Property enhancement of 3D-printed alumina ceramics using vacuum infiltration. *J Mater Process Technol* 2014, **214**: 1301–1306.

[22] Kim JH, Noh HG, Kim US, *et al*. Recent advances in the ink-jet printing ceramic tile using colorant ceramic-ink. *J Korean Ceram Soc* 2013, **50**: 498–503.

[23] Eckel ZC, Zhou C, Martin JH, *et al*. Additive manufacturing of polymer-derived ceramics. *Science* 2016, **351**: 58–62.

[24] Halloran JW. Ceramic stereolithography: Additive manufacturing for ceramics by photopolymerization. *Annu Rev Mater Res* 2016, **46**: 19–40.

[25] Lasgorceix M, Champion E, Chartier T. Shaping by microstereolithography and sintering of macro–micro-porous silicon substituted hydroxyapatite. *J Eur Ceram Soc* 2016, **36**: 1091–1101.

[26] Zanchetta E, Cattaldo M, Franchin G, *et al*. Stereolithography of SiOC ceramic microcomponents. *Adv Mater* 2016, **28**: 370–376.

[27] Franchin G, Maden H, Wahl L, *et al*. Optimization and characterization of preceramic inks for direct ink writing of ceramic matrix composite structures. *Materials* 2018, **11**: 515.

[28] Franchin G, Wahl L, Colombo P. Direct ink writing of ceramic matrix composite structures. *J Am Ceram Soc* 2017, **100**: 4397–4401.

[29] Tekinalp HL, Kunc V, Velez-Garcia GM, *et al*. Highly oriented carbon fiber–polymer composites via additive manufacturing. *Compos Sci Technol* 2014, **105**: 144–150.

[30] Matsuzaki R, Ueda M, Namiki M, *et al*. Three-dimensional printing of continuous-fiber composites by in-nozzle impregnation. *Sci Rep* 2016, **6**: 23058.

[31] Yang CC, Tian XY, Liu TF, *et al*. 3D printing for continuous fiber reinforced thermoplastic composites: Mechanism and performance. *Rapid Prototyp J* 2017, **23**: 209–215.

[32] Chabaud G, Castro M, Denoual C, *et al*. Hygromechanical properties of 3D printed continuous carbon and glass fibre reinforced polyamide composite for outdoor structural applications. *Addit Manuf* 2019, **26**: 94–105.

[33] Mao WG, Wang YJ, Shi J, *et al*. Bending fracture behavior of freestanding $(Gd_{0.9}Yb_{0.1})_2Zr_2O_7$ coatings by using digital image correlation and FEM simulation with 3D geometrical reconstruction. *J Adv Ceram* 2019, **8**: 564–575.

[34] Stepashkin AA, Chukov DI, Senatov FS, *et al*. 3D-printed PEEK-carbon fiber (CF) composites: Structure and thermal properties. *Compos Sci Technol* 2018, **164**: 319–326.

[35] Lewicki JP, Rodriguez JN, Zhu C, *et al*. 3D-printing of meso-structurally ordered carbon fiber/polymer composites

with unprecedented orthotropic physical properties. *Sci Rep* 2017, **7**: 43401.
[36] Lewis JA. Direct-write assembly of ceramics from colloidal inks. *Curr Opin Solid State Mater Sci* 2002, **6**: 245–250.
[37] Compton BG, Lewis JA. 3D-printing of lightweight cellular composites. *Adv Mater* 2014, **26**: 5930–5935.
[38] Ma GW, Li ZJ, Wang L, *et al*. Micro-cable reinforced geopolymer composite for extrusion-based 3D printing. *Mater Lett* 2019, **235**: 144–147.
[39] Mueller J, Raney JR, Shea K, *et al*. Architected lattices with high stiffness and toughness via multicore-shell 3D printing. *Adv Mater* 2018, **30**: 1705001.
[40] Mei H, Yan YK, Feng LP, *et al*. First printing of continuous fibers into ceramics. *J Am Ceram Soc* 2019, **102**: 3244–3255.
[41] Senff L, Labrincha JA, Ferreira VM, *et al*. Effect of nano-silica on rheology and fresh properties of cement pastes and mortars. *Constr Build Mater* 2009, **23**: 2487–2491.
[42] Yu HJ, Jiang YT, Lu YF, *et al*. Quartz fiber reinforced Al_2O_3–SiO_2 aerogel composite with highly thermal stability by ambient pressure drying. *J Non-Cryst Solids* 2019, **505**: 79–86.
[43] Lü Z, Geng HR, Zhang MX, *et al*. Preparation of aluminum borate whisker reinforced aluminum phosphate wave-transparent materials. *Sci Bull* 2008, **53**: 3073–3076.
[44] Sun ZQ, Huang PZ, Gu AJ, *et al*. Novel high-performance wave-transparent aluminum phosphate/cyanate ester composites. *J Appl Polym Sci* 2012, **123**: 1576–1583.
[45] Chen N, Wang HB, Huo JC, *et al*. Preparation and properties of *in situ* mullite whiskers reinforced aluminum chromium phosphate wave-transparent ceramics. *J Eur Ceram Soc* 2017, **37**: 4793–4799.